(Received 31 January 2025, Accepted 1 April 2025, Scheduled 3 April 2025)

Design of Variable Boundary Layer Sliding Mode Observer for Permanent Magnet Synchronous Motor Based on Fuzzy Control

Yu Nan*, Lei Wang, Meng Qi, and Zhi Li

Kaifeng Power Supply Company, State Grid Henan Electric Power Company, Kaifeng 475000, China

ABSTRACT: A novel position-free control strategy for permanent magnet synchronous motors (PMSMs) based on an improved fuzzy sliding mode observer (FSMO) is proposed to enhance the accuracy of rotor position estimation across different speeds. Traditional sliding mode observers (SMOs) employ a single sliding mode control rate, limiting their precision under varying speed conditions. To address this, the proposed FSMO adaptively adjusts the boundary layer thickness based on system stability and speed, effectively suppressing sliding mode chattering under diverse operating conditions. Additionally, a complex coefficient filter is integrated to mitigate the adverse effects of abrupt boundary layer changes on system stability by filtering the back electromotive force (EMF). Furthermore, a phase-locked loop (PLL) is employed to precisely extract and estimate rotor position and speed. Experimental results demonstrate that the proposed FSMO outperforms conventional SMOs and fixed-boundary-layer SMOs, achieving more accurate rotor position and speed estimation across different operating speeds.

1. INTRODUCTION

Permanent magnet synchronous motor (PMSM) has the characteristics of simple structure, high power factor, high efficiency, simple drive control, etc., and has been widely used in new energy vehicles, household appliances, aerospace, and other fields [1, 2]. In aerospace field, with the development of intelligent technology, unmanned aerial vehicle (UAV) has been widely used in various fields such as agriculture, logistics and transportation, aerial photography, national defense and military. The precise control of UAV flight attitude is directly related to the motor control system, but the position sensor required by the traditional PMSM control strategy will increase the UAV load and have high requirements on the operating environment, which limits its application in the UAV field. In order to improve the control performance of PMSM, scholars have conducted extensive research on the position sensorless control strategy of PMSM [3]. The current position sensorless control of PMSM is divided into two categories according to the applicable speed range. The first type is zero low speed control method without position sensor, which mainly includes I/F operation control method [4], low frequency signal injection method [5], high frequency signal injection method [6], etc. The second category is the sensorless control methods of medium and high speed, which mainly include flux estimation method [7], sliding mode observer (SMO) method [8], model reference adaptive method [9], extended Kalman filter method [10], artificial intelligence algorithm [11], etc. Among them, SMO method is widely used in the sensorless control of permanent magnet synchronous motors in medium and high speed scenarios because of its strong robustness, good resistance to external disturbance, and insensitivity to system parameters. However, due to the inherent buffeting problem, the extended back electromotive force (EMF) contains a large number of harmonics, which affects the control accuracy and stability [6].

The processing method of traditional SMO is to carry out low-pass filtering (LPF) on the back EMF, but it will cause the phase shift and amplitude attenuation of the estimated back EMF, and cannot eliminate the ripple component. In [12], a back EMF observer is used instead of a low-pass filter to improve the accuracy of the estimation, and the feedback coefficient is adjusted adaptively. In [13], hyperbolic tangent function is used to replace the symbolic function in traditional SMO to weaken sliding mode buffeting, and a fuzzy SMO control strategy based on two-stage filtering is designed. In [14], a complex coefficient current error term is introduced into the traditional SMO using sigmoid function to solve the problem of estimating the phase delay of the back EMF. In [15], in addition to a smoother surface tangent function, SOGI filter is added to the PLL to solve the phase delay problem, and the angle compensation method based on current discrete error is used to compensate the digital control delay. In [16], the exponential function of fuzzy control is used as the switching function, and an improved sliding mode disturbance observer is constructed as a feedforward compensator to optimize the dynamic performance of the improved observation system by compensating the Q-axis current.

However, the above control strategy has poor adaptability in the case of variable speed, and it is difficult to maintain the weakening effect on sliding mode buffeting in the working environment where the motor speed of the UAV needs to be adjusted frequently, which reduces the control accuracy and stability of the system. Considering that unmanned aircraft system

* Corresponding author: Yu Nan (nanyu12024@163.com).

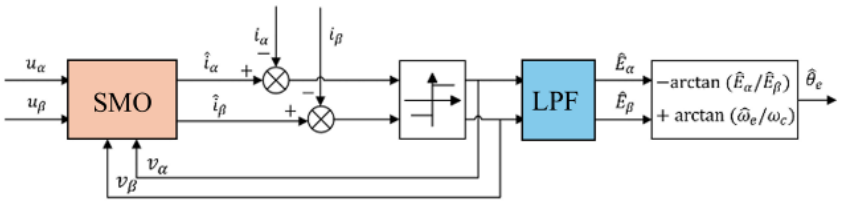

FIGURE 1. Block diagram of traditional SMO.

is a complex nonlinear system, its control is faced with external dynamic interference and uncertainty. Based on the above literature, this paper improves the sliding mode surface function and control rate, and uses fuzzy control to automatically adjust the boundary layer of the input function, so that the system can adaptively improve the control accuracy and effectively suppress sliding mode buffering. By introducing a complex coefficient filter instead of the traditional low-pass filter, the filtering performance and position observation accuracy are improved, and the speed and position information of the rotor is accurately extracted by using a PLL. An experimental platform based on dSPACE is built, and the advantages and effectiveness of the proposed control strategy are verified through comparative experiments.

2. PMSM POSITIONLESS CONTROL PRINCIPLE BASED ON SMO

The sensorless control system of PMSM based on traditional SMO estimates the back EMF according to voltage and current, and then obtains the rotor position and speed by inverse tangent function and differentiation.

2.1. Mathematical Model of PMSM

The table mount PMSM mathematical model in the $\alpha\beta$ stationary coordinate frame can be expressed as

$$\begin{bmatrix} u_\alpha \\ u_\beta \end{bmatrix} = \begin{bmatrix} R_q + pL_q & 0 \\ 0 & R_q + pL_q \end{bmatrix} \begin{bmatrix} i_\alpha \\ i_\beta \end{bmatrix} + \begin{bmatrix} E_\alpha \\ E_\beta \end{bmatrix}, \quad (1)$$

where u_α, u_β are the stator voltages; i_α, i_β are the stator currents; E_α, E_β are the back EMF signals in the $\alpha\beta$ frame, respectively; L_s is the winding inductance; R_s is the winding resistance; p is the differential operator. The back EMF equation can be described as:

$$\begin{bmatrix} E_\alpha \\ E_\beta \end{bmatrix} = \omega_e \psi_f \begin{bmatrix} -\sin\theta_e \\ \cos\theta_e \end{bmatrix}, \quad (2)$$

where ω_e is the electrical angular velocity; ψ_f is the flux linkage of the PMSM; θ_e is the rotor electrical position.

In order to facilitate the observation of extended back EMF by SMO, Equation (1) is rewritten as the state equation of current:

$$p\begin{bmatrix} i_\alpha \\ i_\beta \end{bmatrix} = -\frac{R_s}{L_s}\begin{bmatrix} i_\alpha \\ i_\beta \end{bmatrix} + \frac{1}{L_s}\begin{bmatrix} u_\alpha \\ u_\beta \end{bmatrix} - \frac{1}{L_s}\begin{bmatrix} E_\alpha \\ E_\beta \end{bmatrix}. \quad (3)$$

2.2. Design of Traditional SMO

According to the mathematical model of PMSM, the design observer is

$$p\begin{bmatrix} \hat{i}_\alpha \\ \hat{i}_\beta \end{bmatrix} = -\frac{R_s}{L_s}\begin{bmatrix} \hat{i}_\alpha \\ \hat{i}_\beta \end{bmatrix} + \frac{1}{L_s}\begin{bmatrix} u_\alpha \\ u_\beta \end{bmatrix} - \frac{1}{L_s}\begin{bmatrix} v_\alpha \\ v_\beta \end{bmatrix}, \quad (4)$$

where $\hat{i}_\alpha, \hat{i}_\beta$ are the estimated currents, respectively; v_α, v_β are the control input to the observer, respectively.

By making the difference between Equation (3) and Equation (4), the error equation of stator current can be obtained as:

$$p\begin{bmatrix} \tilde{i}_\alpha \\ \tilde{i}_\beta \end{bmatrix} = -\frac{R_s}{L_s}\begin{bmatrix} \tilde{i}_\alpha \\ \tilde{i}_\beta \end{bmatrix} + \frac{1}{L_s}\begin{bmatrix} E_\alpha - v_\alpha \\ E_\beta - v_\beta \end{bmatrix}, \quad (5)$$

where $\tilde{i}_\alpha = \hat{i}_\alpha - i_\alpha, \tilde{i}_\beta = \hat{i}_\beta - i_\beta$ are current observation errors, respectively.

The sliding mode control rate is designed as:

$$\begin{bmatrix} v_\alpha \\ v_\beta \end{bmatrix} = k\begin{bmatrix} \mathbf{sgn}(\hat{i}_\alpha - i_\alpha) \\ \mathbf{sgn}(\hat{i}_\beta - i_\beta) \end{bmatrix}, \quad (6)$$

where k is the sliding mode gain.

It can be seen from Equation (2) that the estimated position information of the rotor can be obtained through the arctangent function, that is,

$$\hat{\theta}_{eq} = -\arctan(\hat{E}_\alpha/\hat{E}_\beta). \quad (7)$$

Since the control quantity is a discontinuous high frequency switching signal, high order harmonics need to be filtered out by LPF. At this time, the extended back EMF will produce phase delay, which needs to be compensated according to the estimated speed and LPF cutoff frequency, that is,

$$\hat{\theta}_e = \hat{\theta}_{eq} + \arctan(\hat{\omega}_e/\omega_c). \quad (8)$$

where $\hat{\omega}_e$ is the estimated speed, which can be obtained by differentiating the estimated position; ω_c is the LPF cutoff frequency.

The principle of traditional sliding mode observer is shown in Fig. 1.

2.3. Estimation Accuracy of Traditional SMO at Different Speeds

Simulation experiments were set up to observe the estimated position error and estimated speed error of traditional SMO at different speeds. As shown in Fig. 2, with the increase of motor speed, the estimated position error and speed error of traditional SMO gradually increase, and the system cannot be adjusted adaptively to maintain the estimated progress.

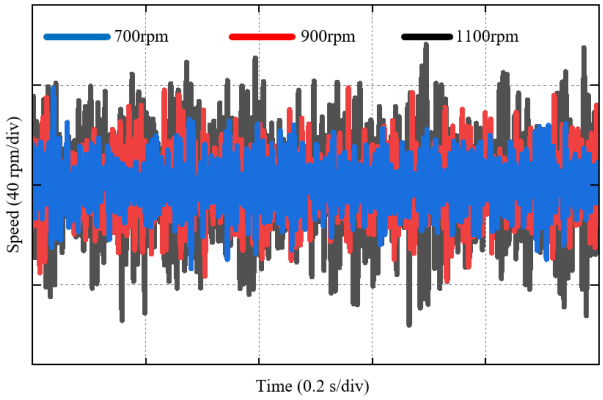

FIGURE 2. Comparison of speed errors.

3. DESIGN OF VARIABLE BOUNDARY LAYER FSMO FOR PMSM

3.1. Improved FSMO Principles

To solve the above problems, an improved FSMO is proposed, and its schematic diagram is shown in Fig. 3.

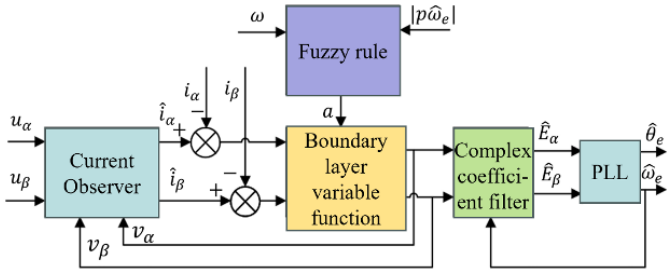

FIGURE 3. Improved FSMO structure block diagram.

By changing the switching function of the sliding mode controller to the variable function of the boundary layer and designing fuzzy control rules, the boundary layer of the improved switching function can change adaptively with the change of the working condition, so as to realize the adaptive adjustment of the estimation accuracy of the sliding mode observer. In order to avoid the introduction of harmonic interference due to the change of boundary layer in real time, the harmonic component in the back EMF is filtered by complex coefficient filter, and the estimated rotor position and speed are accurately extracted by PLL structure. Fig. 4 shows the block diagram of PMSM sensorless control system based on improved FSMO.

3.2. Design of FSMO

The switching function of traditional SMO uses a non-smooth switching function, which leads to high-frequency buffeting problems. Meanwhile, the use of LPF to extract continuous extended back EMF estimates will cause amplitude changes and phase delays of the extended back EMF estimates [17]. In order to solve the chattering problem of traditional SMO, the continuous switching function sigmoid $(\cdot)$ at zero point is used instead of the sgn $(\cdot)$ function, which can effectively weaken the high-frequency chattering of sliding mode.

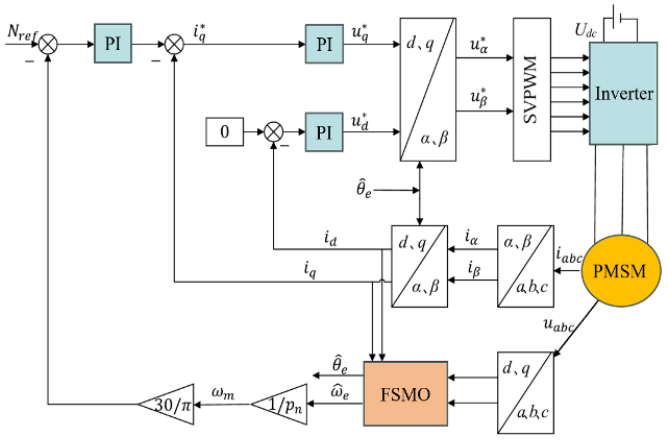

FIGURE 4. Block diagram of PMSM sensorless control system based on FSMO.

The expression for the sigmoid $(\cdot)$ function is:

$$\textbf{sigmoid}(x) = \frac{2}{1+e^{-ax}} - 1, \tag{9}$$

where a is a coefficient, and its size affects the convergence property of the function.

In order to prove the stability of the system, the sliding mode surface is chosen as

$$\begin{bmatrix} s_\alpha \\ s_\beta \end{bmatrix} = \begin{bmatrix} \tilde{i}_\alpha \\ \tilde{i}_\beta \end{bmatrix} = \begin{bmatrix} \hat{i}_\alpha - i_\alpha \\ \hat{i}_\beta - i_\beta \end{bmatrix}. \tag{10}$$

Define the Lyapunov function as

$$V = \frac{1}{2} s s^T. \tag{11}$$

According to Lyapunov stability theorem, the system stability condition is $\dot{V} < 0$. Take the derivative of Equation (11) and get

$$\dot{V} = \dot{s} s^T < 0. \tag{12}$$

By combining the current Equations (3) and (4) in the $\alpha\beta$ stationary coordinate frame, the derivative of current observation error can be expressed as

$$\begin{cases} \dot{s}_\alpha = \dot{\hat{i}}_\alpha - \dot{i}_\alpha \\ = -\frac{R_s}{L_s}(\hat{i}_\alpha - i_\alpha) + \frac{1}{L_s} e_\alpha - \frac{1}{L_s} k \cdot \textbf{sigmoid}(\tilde{i}_\alpha) \\ \dot{s}_\beta = \dot{\hat{i}}_\beta - \dot{i}_\beta \\ = -\frac{R_s}{L_s}(\hat{i}_\beta - i_\beta) + \frac{1}{L_s} e_\beta - \frac{1}{L_s} k \cdot \textbf{sigmoid}(\tilde{i}_\beta) \end{cases}. \tag{13}$$

Substituting Equation (13) with stability condition (12), the inequality can be obtained as

$$[\tilde{i}_\alpha \ \tilde{i}_\beta] \begin{bmatrix} -\frac{R_s}{L_s}(\hat{i}_\alpha - i_\alpha) + \frac{1}{L_s}\left[e_\alpha - k \cdot \textbf{sigmoid}(\tilde{i}_\alpha)\right] \\ -\frac{R_s}{L_s}(\hat{i}_\beta - i_\beta) + \frac{1}{L_s}\left[e_\beta - k \cdot \textbf{sigmoid}(\tilde{i}_\beta)\right] \end{bmatrix} < 0. \tag{14}$$

From this, the sliding mode gain satisfying the inequality conditions can be derived as

$$k > \max(|E_\alpha|, |E_\beta|). \tag{15}$$

When this condition is satisfied, the system can carry out sliding mode motion and eventually stabilize around the equilibrium point. In this case, the sliding mode control rate can be expressed as

$$\begin{bmatrix} v_\alpha \\ v_\beta \end{bmatrix} = k \begin{bmatrix} \textbf{sigmoid}(\hat{i}_\alpha - i_\alpha) \\ \textbf{sigmoid}(\hat{i}_\beta - i_\beta) \end{bmatrix}. \tag{16}$$

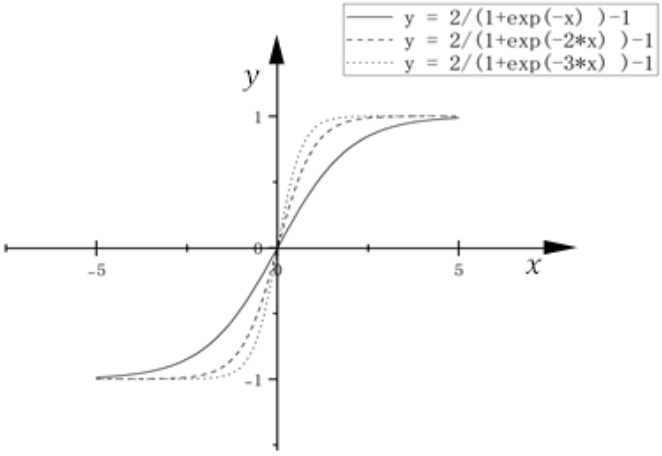

FIGURE 5. Switching function under different a.

As can be seen in Fig. 5, when $|x|$ is greater than a certain range, sigmoid $(\cdot)$ function and sgn $(\cdot)$ function have the same effect. When $|x|$ is less than a certain range, sliding mode control can be approximated as linear control, thus reducing system buffeting and enhancing stability. This range is the boundary layer, and the thickness of the boundary layer can be changed by changing the size of a. The smaller the boundary layer is, the faster the system can enter the sliding mode, but at the same time the sliding mode buffeting will intensify. The larger the boundary layer is, the sliding mode buffeting will weaken, but the system cannot reach the sliding mode surface, and the increase of the estimated current error will reduce the control accuracy of the system. Therefore, to achieve both low sliding mode buffeting and high steady-state accuracy, it is necessary to select the boundary layer reasonably. The selection methods of boundary layer in the past often rely on experience, and a large amount of work is required to determine the appropriate boundary layer. At the same time, it is difficult for the fixed sliding mode boundary layer to achieve the optimal performance of the observer, because the change of the motor speed will lead to the change of the back EMF. Combined with Equation (11), it can be seen that the boundary layer should be adjusted in time to adapt to the change of the estimated current error, so as to weaken the sliding mode buffeting as much as possible and reduce the decrease in control accuracy caused by changing the switching function.

In this paper, while the dynamic performance is considered, the absolute value of the derivative of the estimated velocity is taken as the measure of buffering degree, and the influence of the given velocity on sliding mode buffeting is observed in combination with the experiment. The following fuzzy rules are established between the two and a.

When the system buffeting is considerable, the control becomes smoother by augmenting the thickness of the boundary layer. When the system buffeting is minor, the thickness of the boundary layer is decreased to enhance the control accuracy. When the given speed is elevated, the lower limit of the boundary layer range is increased to guarantee that the buffeting effect is mitigated. The fuzzy rules are presented in Tables 1 and 2.

TABLE 1. Fuzzy rule base.

a		$\lvert p\hat{\omega}_e \rvert$			
		Z	PS	PM	PB
ω	Z	PB	PM	PS	Z
	PS	PM	PS	PS	Z
	PM	PS	PS	Z	Z
	PB	PS	Z	Z	Z

TABLE 2. Rule base reference value.

Symbol	$\lvert p\hat{\omega}_e \rvert_Z$	$\lvert p\hat{\omega}_e \rvert_{PS}$	$\lvert p\hat{\omega}_e \rvert_{PM}$	$\lvert p\hat{\omega}_e \rvert_{PB}$
Value	[0 400]	[400 1000]	[1000 5000]	[5000 10000]
Symbol	a_Z	a_{PS}	a_{PM}	a_{PB}
Value	[0.1 0.5]	[0.5 1]	[1 2]	[2 3]
Symbol	ω_Z	ω_{PS}	ω_{PM}	ω_{PB}
Value	[0 500]	[500 1000]	[1000 1500]	[1500 2000]

3.3. Design of Complex Coefficient Filter

After the traditional SMO low-pass filter filters back EMF, the amplitude of the obtained back EMF will be attenuated to a certain extent because of the characteristics of LPF, and it can hardly filter the lower harmonics, such as the 5th and 7th harmonics, resulting in inherent phase delay. In order to solve this problem, angle compensation is usually added, but it is difficult to completely compensate the error. In order to avoid introducing additional error factors, this paper uses a first-order complex coefficient filter instead of the traditional LPF to filter harmonic interference in the estimated back EMF as

$$G(s) = \frac{\omega_c}{s - j\omega_r + \omega_c}, \tag{17}$$

where ω_c is the cut-off frequency; ω_r is the central frequency.

In actual operation, the change of the working speed of the motor will result in the change of the estimated back EMF frequency. Therefore, in order to satisfy the good filtering performance of the system under different motor speeds and realize the adaptability of the complex coefficient filter, the obtained estimated SMO speed is taken as the center frequency of the complex coefficient filter, and the cutoff frequency is taken as the product of the estimated speed and a related factor, which is expressed as

$$\begin{cases} \omega_r = \hat{\omega}_e \\ \omega_c = k_a \omega_r \end{cases}. \tag{18}$$

wherein, k_a represents the filter factor. The larger the value of k_a is, the higher the cutoff frequency of the system becomes,

and the better the dynamic performance is; however, the filtering performance will deteriorate. Conversely, the smaller the value of k_a is, the better the filtering performance of the system is, but the dynamic performance will be compromised. The structure block diagram of the complex coefficient filter is shown in Fig. 6.

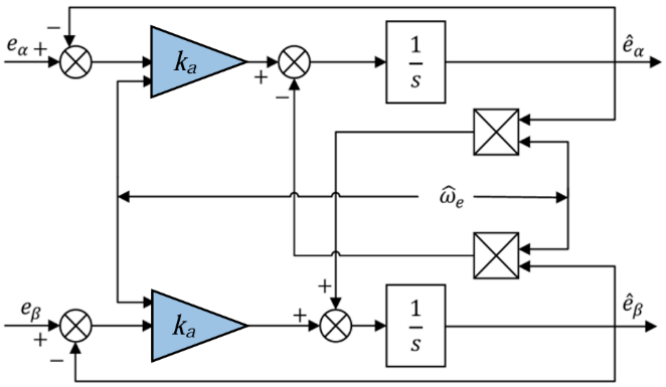

FIGURE 6. Structure block diagram of complex coefficient filter.

The ideal complex coefficient filter has unit-gain and zero phase shift at the center frequency and deep attenuation at other frequencies, which can effectively suppress the amplitude and phase shift. Using the estimated rotational speed of SMO as the center frequency of the complex coefficient filter, the obtained adaptive complex coefficient filter can change the center frequency of the filter according to the frequency change of the estimated extended back EMF and improve the position estimation accuracy of the system.

3.4. Design of PLL

Traditional SMO usually uses the inverse tangent function and differential calculation to calculate the position and speed of the rotor. Although the method has good dynamic performance, the introduced arctangent function and division operation will amplify the error caused by high frequency jitter, bring a lot of noise to the system, and interfere with the steady-state accuracy. The PLL can automatically track the output frequency according to the frequency and phase of the input signal. At the same time, PLL has good anti-interference performance and small static error, which can significantly improve the accuracy of position estimation and rotational speed estimation. Therefore, this paper uses PLL to extract the position and speed of the rotor. Its structure block diagram is shown in Fig. 7.

Establish an equation as

$$k = (L_d - L_q)(\omega_e i_d - p i_q) + \hat{\omega}_e \psi_f. \tag{19}$$

According to Fig. 7, an equation can be established as

$$\begin{aligned} \Delta E &= -\hat{E}_\alpha \cos\hat{\theta}_e - \hat{E}_\beta \sin\hat{\theta}_e \\ &= k \sin\theta_e \cos\hat{\theta}_e - k \cos\theta_e \sin\hat{\theta}_e \\ &= k \sin\left(\theta_e - \hat{\theta}_e\right) \approx k\left(\theta_e - \hat{\theta}_e\right). \end{aligned} \tag{20}$$

In summary, compared with the traditional SMO, the new switching function is adopted; the complex coefficient filter is used to replace the traditional LPF; and the PLL is used to extract the rotor position and speed. Although the algorithm complexity is increased to a certain extent, it has a good effect on improving the stability and observation accuracy of the system, as well as improving the dynamic performance of the system.

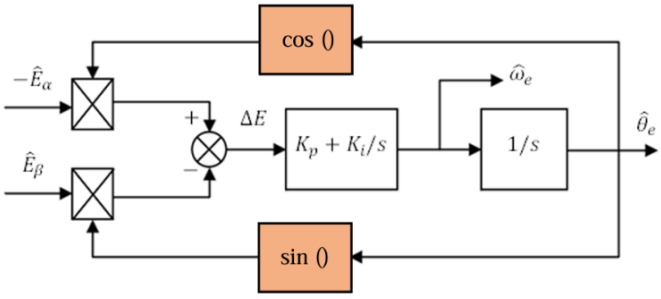

FIGURE 7. PLL block diagram.

4. EXPERIMENTAL RESULTS

In order to verify the effectiveness of the above method, an experimental platform for the sensorless control system of PMSM based on traditional SMO and improved FSMO was built through dSPACE, and the Pulse Width Modulation (PWM) switching frequency was 10 kHz, as shown in Fig. 8. Sampling motor parameters are shown in Table 3.

Figure 9 shows the estimated extended back EMF waveform of the two synovial observers at steady state. It can be seen that the traditional SMO using LPF is difficult to achieve the ideal estimated back EMF waveform; the harmonic content is

TABLE 3. Experimental motor parameters.

Parameter	Value	Unit
the number of pole pairs p	3	-
stator winding resistant R_s	3.03	(Ω)
stator inductance L_s(mH)	7.9	mH
rotational inertia J	3.9	kg(kg·m^2)m^2

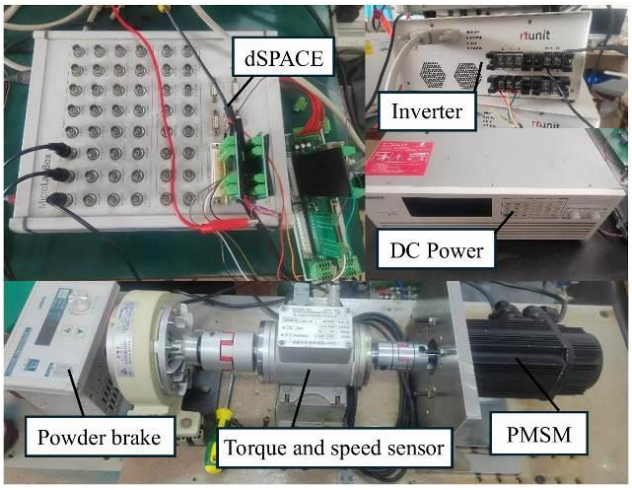

FIGURE 8. Experimental platform.

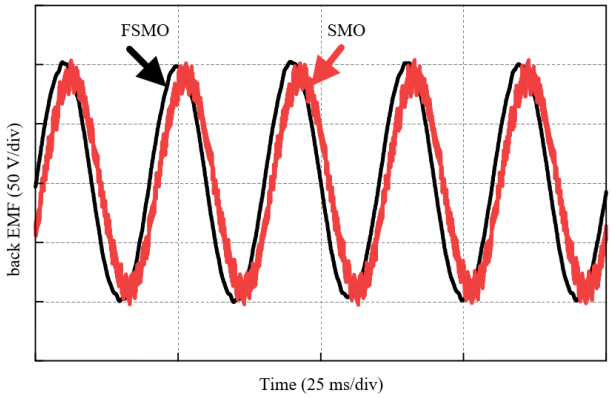

FIGURE 9. Comparison of estimated extended back EMF.

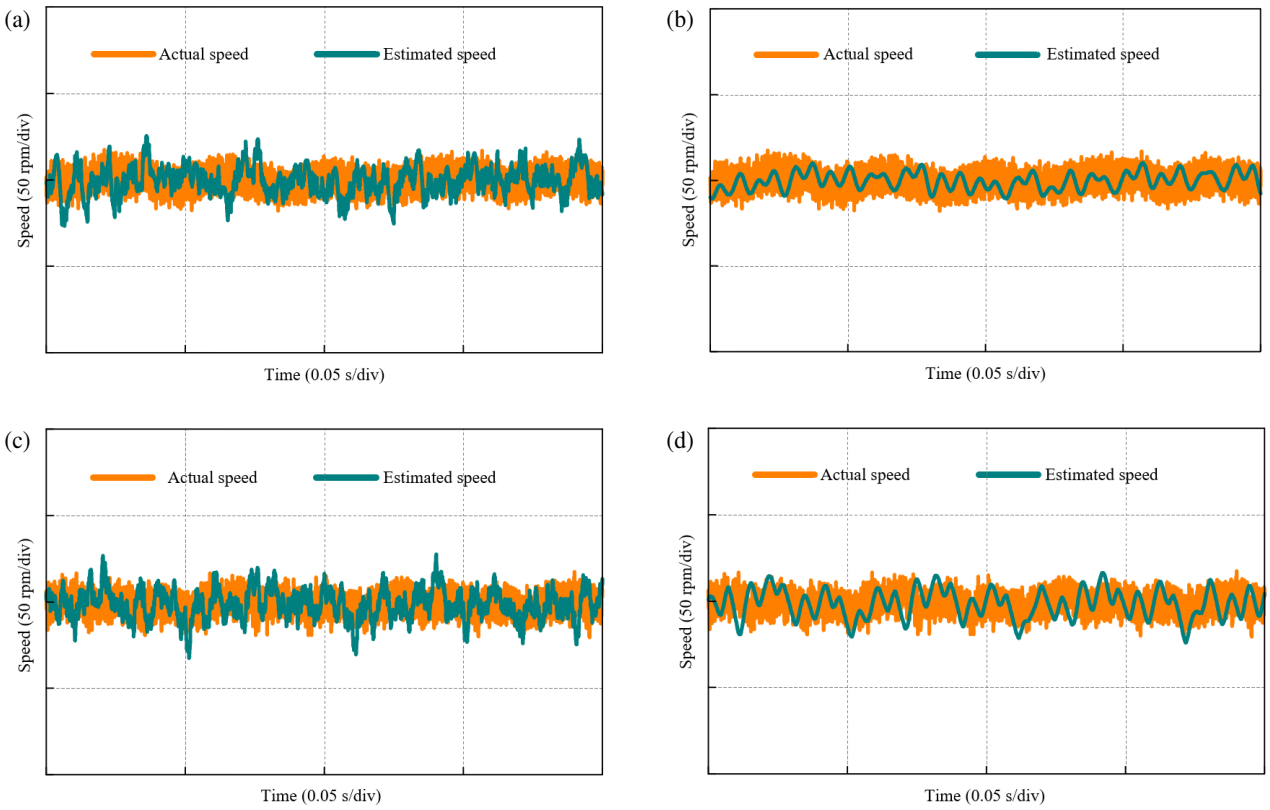

FIGURE 10. Experimental results of rotational speed. (a) Traditional SMO estimated speed and actual speed at 500 rpm. (b) Improved FSMO estimated speed and actual speed at 500 rpm. (c) Traditional SMO estimated speed and actual speed at 1000 rpm. (d) Improved FSMO estimated speed and actual speed at 1000 rpm.

large; the waveform sine degree is poor. The improved FSMO has obvious suppression effect on harmonic estimation of back EMF, better sinusoidal waveform, and reduces the influence of harmonic on the control system.

Next, verify the operation effect of the improved FSMO algorithm at different steady-state speeds. As shown in Fig. 10, under 500 rpm and 1000 rpm, the maximum speed errors estimated by the traditional SMO are about 26.7 rpm and 33.7 rpm, while the maximum speed errors estimated by the improved FSMO are about 10.5 rpm and 18.6 rpm. The speed error is reduced by 60.67% and 44.81%, respectively.

The position observation accuracy of the improved FSMO algorithm is compared to the traditional SMO and verified. As shown in Fig. 11, under the working conditions of 500 rpm and 1000 rpm, the maximum position errors estimated by the improved FSMO are 0.1 rad and 0.25 rad, while the maximum position errors estimated by the traditional SMO are 0.4 rad and 0.8 rad. According to the comparison, the position error of the improved FSMO algorithm is reduced by 75% and 68.75%, respectively.

In summary, it can be discerned that the enhanced FSMO under diverse working conditions exhibits smaller speed error and

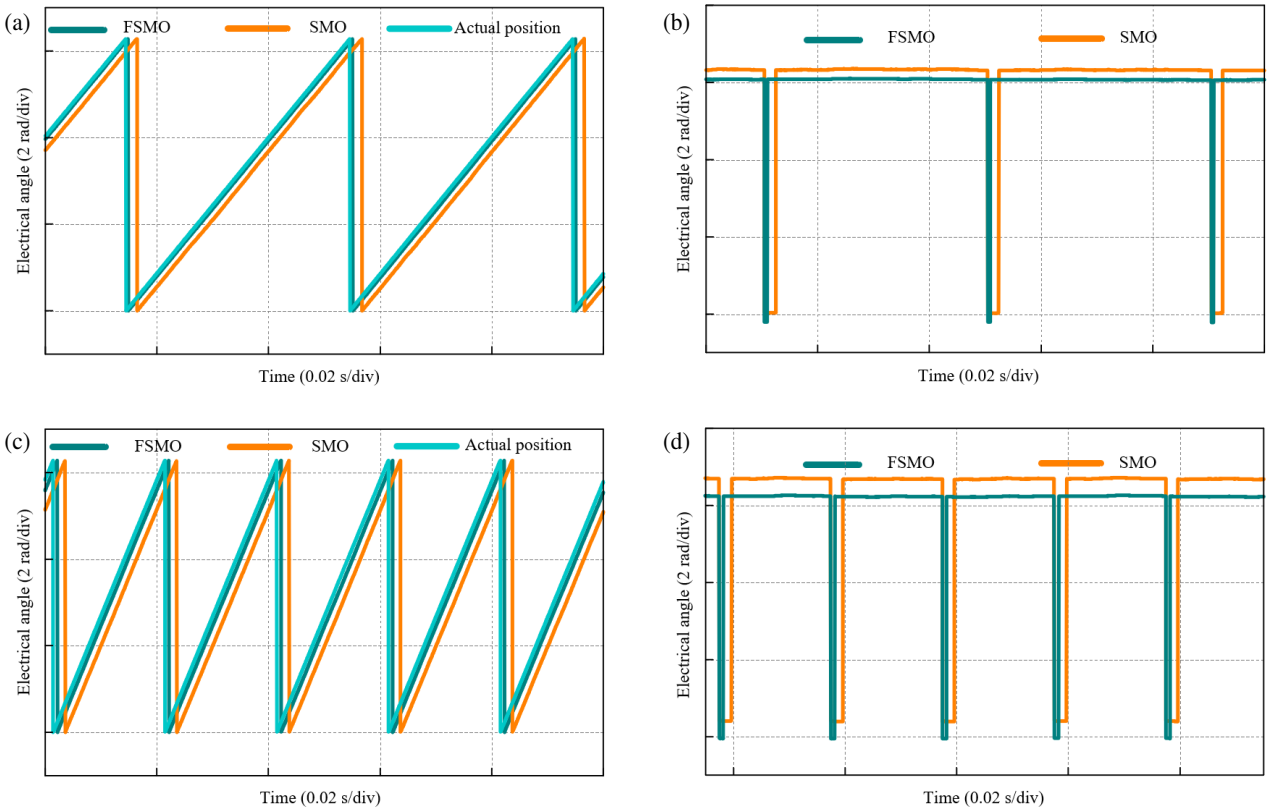

FIGURE 11. Experimental results of rotor position. (a) Estimated and actual rotor position at 500 rpm. (b) Comparison of estimated position errors of rotors at 500 rpm. (c) Estimated and actual rotor position at 1000 rpm. (d) Comparison of estimated position errors of rotors at 1000 rpm.

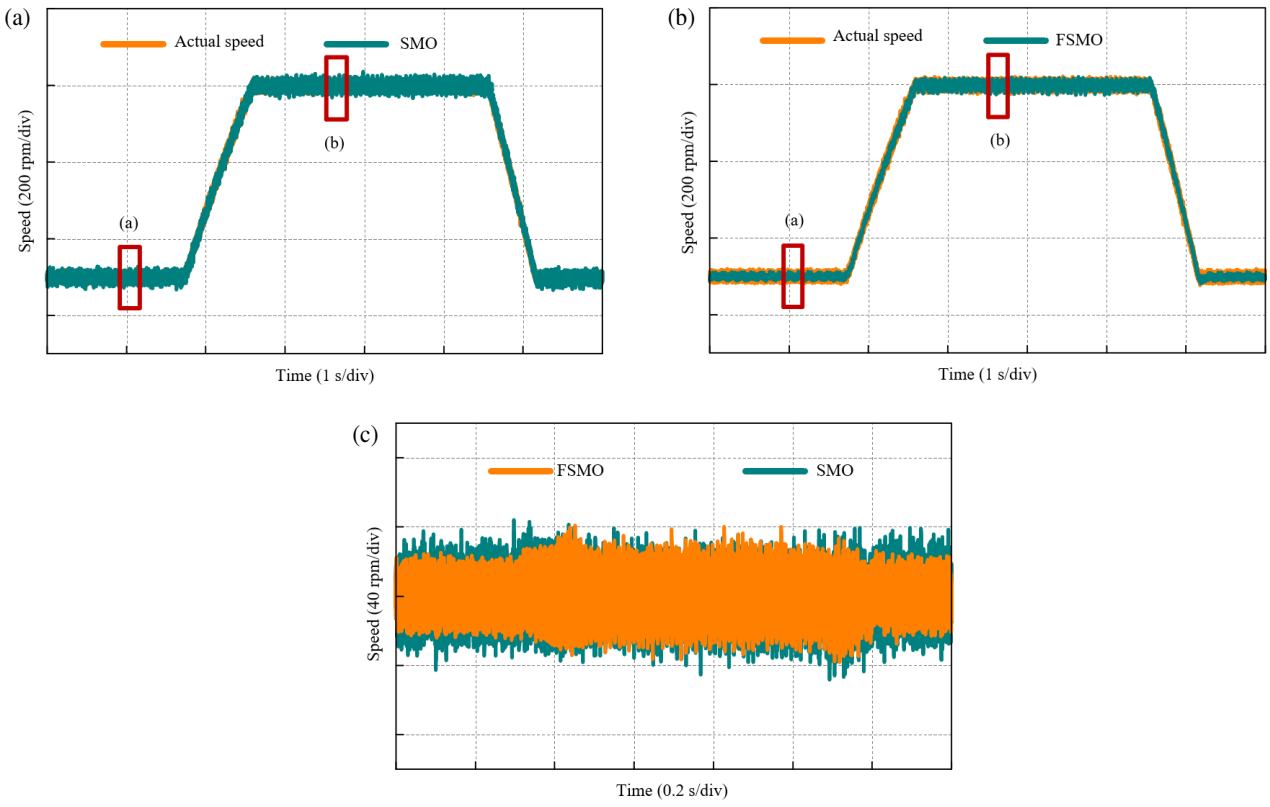

FIGURE 12. Experimental results under speed mutation. (a) Traditional SMO estimated speed and actual speed. (b) Improved FSMO estimated speed and actual speed. (c) Comparison of estimated speed errors.

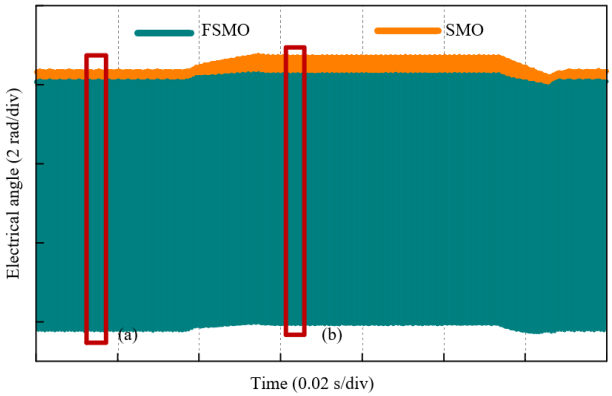

FIGURE 13. Comparison of estimated positions.

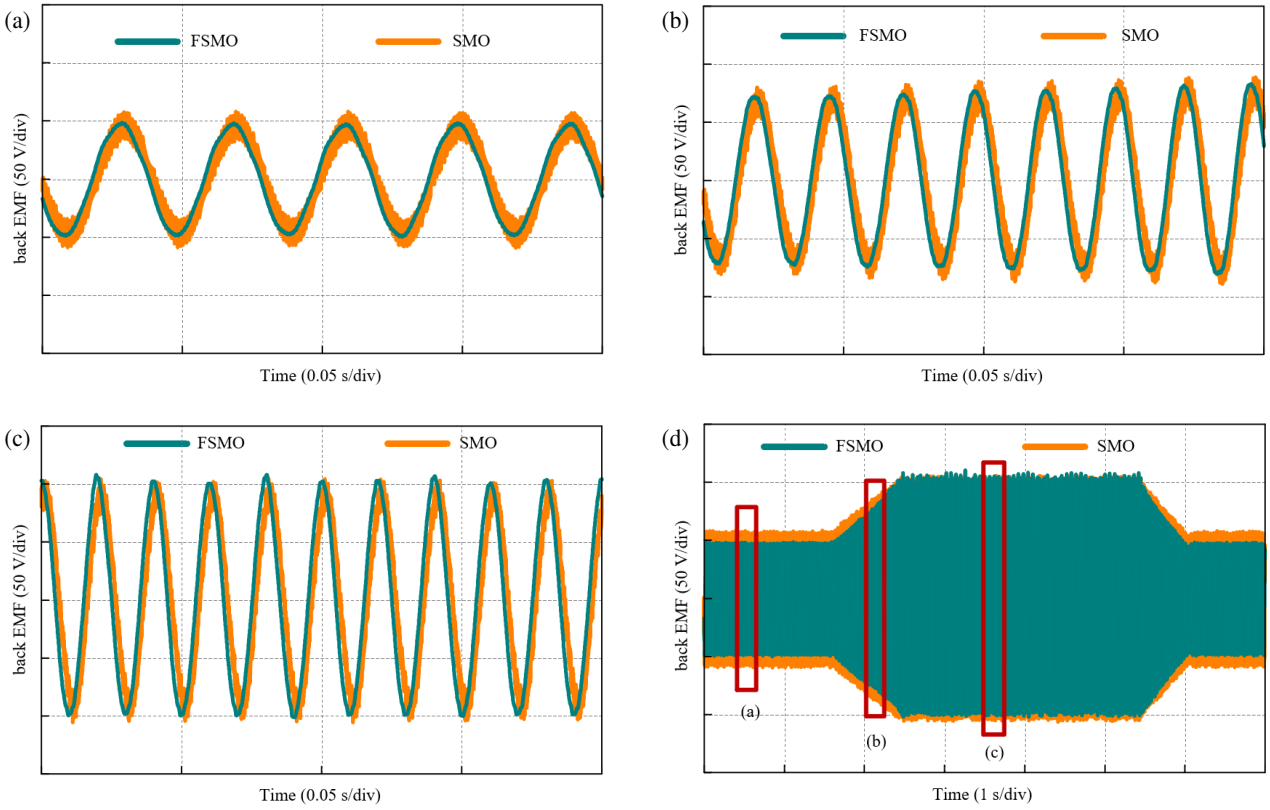

FIGURE 14. Back EMF at different speeds.

higher position estimation accuracy, thereby enhancing the stability and accuracy of the system. Its steady-state performance is significantly superior to that of the traditional SMO, and it is capable of adapting to the working scenarios with frequent variations in working conditions.

In order to verify the dynamic performance of the system, the speed mutation experiment was carried out. As can be seen from Fig. 12, when the speed suddenly increases from 500 rpm to 1000 rpm and then decreases to 500 rpm, the estimated speed of the improved SMO can reliably follow the actual speed on the whole, and the estimated speed error is smaller than that of the traditional SMO.

As evident from Fig. 13, during the process of sudden speed change, the improved estimated position of SMO attains stability more rapidly and exhibits superior dynamic performance. Simultaneously, the steady-state fluctuation of the estimated position of the improved FSMO is approximately 0.15 rad, whereas that of the traditional SMO is about 0.4 rad. This verifies that the improved FSMO is capable of maintaining a high position estimation accuracy under the working condition of frequent speed variations.

By analyzing the waveforms of the back EMF during sudden changes in rotational speed as shown in Fig. 14, it is evident that the back EMF waveforms of the improved FSMO exhibit lower harmonic distortion and higher sinusoidal purity across various rotational speeds. This indicates superior estimation accuracy and faster convergence of the back EMF, thereby further vali-

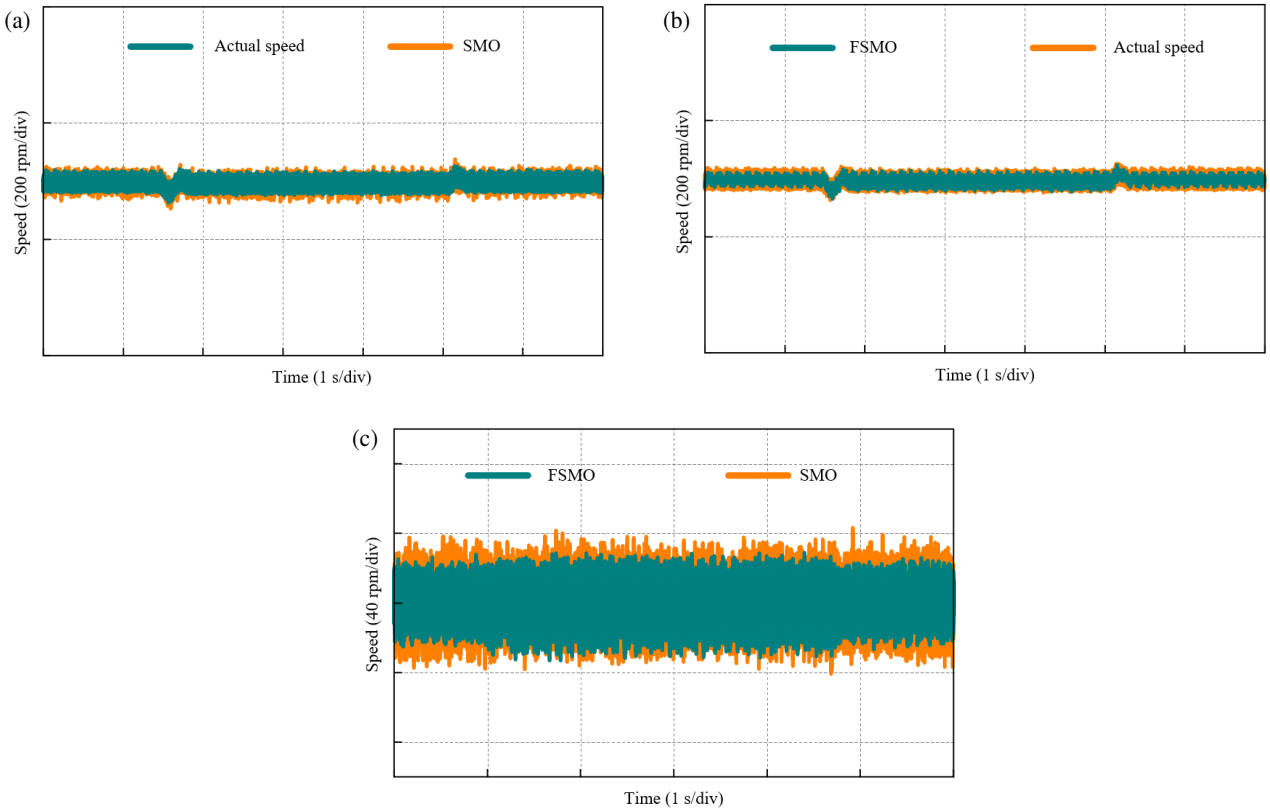

FIGURE 15. Experimental results under load mutation. (a) Traditional SMO estimated speed and actual speed. (b) Improved FSMO estimated speed and actual speed. (c) Comparison of estimated position errors of rotors.

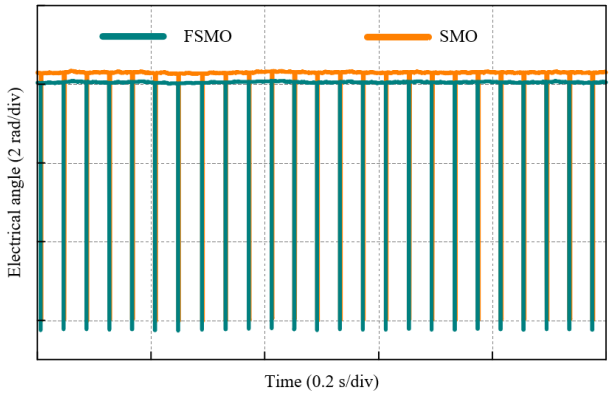

FIGURE 16. Estimated position error under load mutation.

dating the enhanced steady-state and dynamic performance of the improved FSMO.

However, with the increase of rotational speed, the stability of the back EMF waveform observed by the improved FSMO decreases significantly. Although the harmonic content of the back EMF waveform is still smaller than that observed by the traditional SMO, the amplitude fluctuation has increased significantly. This indicates that the improved FSMO will no longer have high estimation accuracy and stability if the given speed is continued to be increased. Therefore, in order to maintain the control accuracy under different conditions, the reference values of the fuzzy rule base need to be readjusted according to the given parameters and experiments, so as to ensure that the control strategy has good control performance.

Next, the performance of the system under sudden load change is verified, and a $2\,\mathrm{N}\cdot\mathrm{m}$ load is abruptly increased and decreased during operation. As depicted in Fig. 15, the steady-state fluctuation of the improved FSMO is approximately 66.7 rpm, while that of the traditional SMO is about 93.3 rpm.

As shown in Fig. 16, the estimated position of the improved SMO and traditional SMO basically did not change in the case of sudden load change. Combined with the experimental results of speed estimation under load sudden change, it can be seen that the improved SMO can better adapt to the interfer-

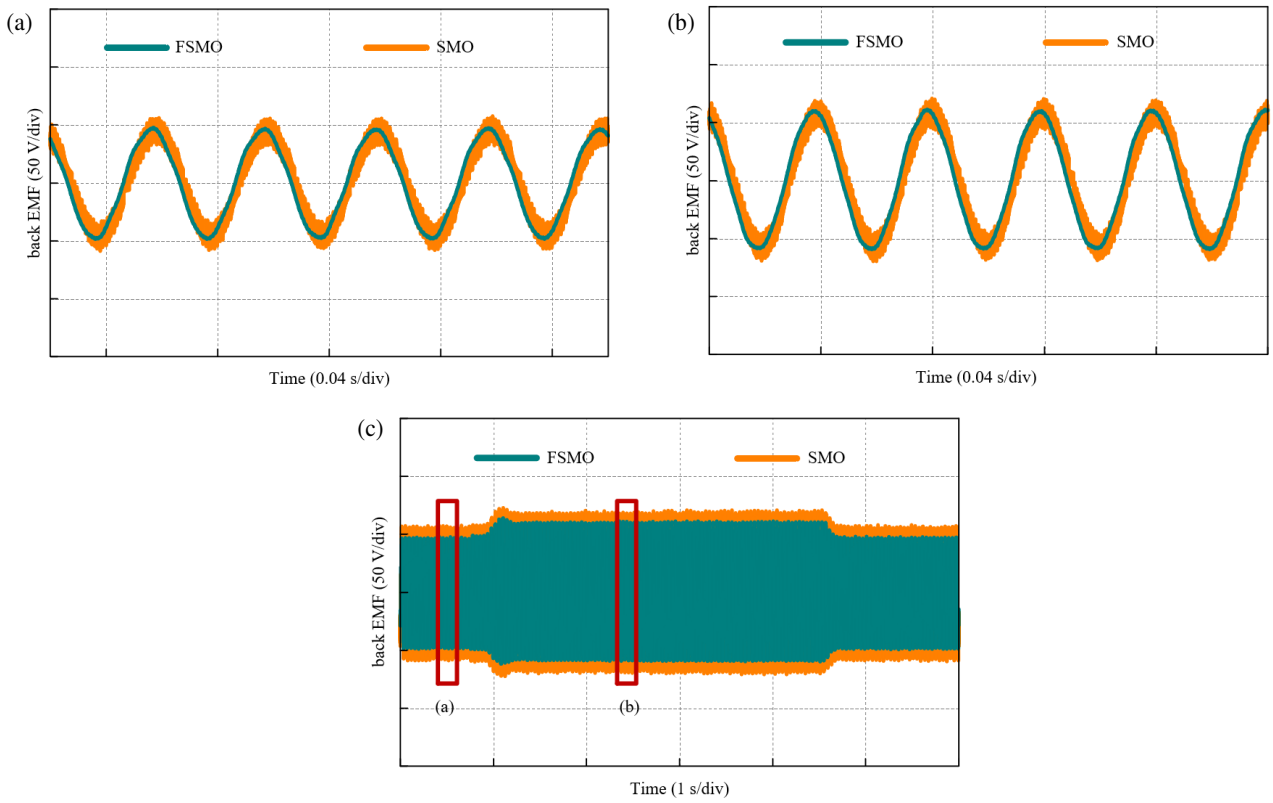

FIGURE 17. Back EMF under load mutation.

ence caused by load sudden change. Fig. 17 also verifies the anti-jamming capability of the improved SMO.

5. CONCLUSION

This paper presents a sensorless control method of permanent magnet synchronous motor with an improved sliding mode observer. The method realizes the adaptive change of the boundary layer of the switching function by using the improved FSMO of fuzzy control and takes into account the steady-state error and sliding mode buffeting suppression. The complex coefficient filter is used to replace the traditional LPF, which can effectively filter out the harmonics in the back EMF and reduce the phase deviation. At the same time, the PLL with high robustness is used to further improve the accuracy of speed and position observation. The experimental results show that compared with the traditional SMO, the proposed method can better reduce the speed fluctuation and anti-EMF harmonic disturbance, thus improving the speed observation accuracy by about 50% and the position observation accuracy by about 60%, and has better dynamic response performance, which has certain reference value for practical engineering applications. At the same time, the control strategy is expected to be applied to industrial automation and intelligent transportation.

For future research, further optimization of the fuzzy control strategy will be explored to enhance the adaptability of the FSMO under varying operating conditions. Moreover, experimental validation in more complex and industrial environments will help assess the robustness and feasibility of the approach in real-world scenarios.

ACKNOWLEDGEMENT

This work was supported in part by State Grid Henan Electric Power Company Technology Project (521790240006).

REFERENCES

[1] Wang, L., Z.-Q. Zhu, H. Bin, and L. M. Gong, "Current harmonics suppression strategy for PMSM with nonsinusoidal back-EMF based on adaptive linear neuron method," *IEEE Transactions on Industrial Electronics*, Vol. 67, No. 11, 9164–9173, Nov. 2020.

[2] Zhang, Y., J. Jin, and L. Huang, "Model-free predictive current control of PMSM drives based on extended state observer using ultralocal model," *IEEE Transactions on Industrial Electronics*, Vol. 68, No. 2, 993–1003, Feb. 2021.

[3] Behera, A. K., S. Mondal, and B. Bandyopadhyay, "A decoupled design of a robust sliding mode observer," *Automatica*, Vol. 148, 110799, 2023.

[4] Zhao, Y. and B. Ning, "Sensorless starting of permanent magnet synchronous motor based on I/F control," *Modular Machine Tool & Automatic Manufacturing Technique*, No. 7, 79–82, 2023.

[5] Zhou, T. and Q. Jiang, "Overview of sensorless control technology for full speed range permanent magnet synchronous motors," *Electronic Science & Technology*, Vol. 34, No. 4, 11, 2021.

[6] Yan, B., J. Liu, Y. Liang, *et al.*, "Review on control technology of position-sensorless permanent-magnet synchronous motor," *Automation & Instrumentation*, Vol. 35, No. 10, 83–87, 2020.

[7] Wang, K., G. Wang, G. Zhang, Q. Wang, B. Li, and D. Xu, "ESO-based robust hybrid flux observer with active flux error estimation for position sensorless PMa-SynRM drives," *IEEE Transactions on Transportation Electrification*, Vol. 11, No. 1, 2049–2060, 2024.

[8] Zuo, Y., C. Lai, and K. L. V. Iyer, "A review of sliding mode observer based sensorless control methods for PMSM drive," *IEEE Transactions on Power Electronics*, Vol. 38, No. 9, 11 352–11 367, Sep. 2023.

[9] Dong, X., H. Wei, *et al.*, "Parameter identification of permanent magnet synchronous motor based on improved model reference adaptive system," *Control Theory & Applications*, Vol. 37, No. 9, 1983–1988, 2020.

[10] Zhou, G., L. Sun, L. Qian, and Q. Zou, "Sensorless predictive control with fusion position estimation technology for PMSM drives," *IEEE Transactions on Transportation Electrification*, Vol. 10, No. 3, 5026–5036, Sep. 2024.

[11] Novak, Z., "Confidence weighted learning entropy for fault-tolerant control of a PMSM with a high-resolution hall encoder," *IEEE Transactions on Industrial Electronics*, Vol. 71, No. 5, 5176–5186, May 2024.

[12] Liu, Z., M. Du, and K. Wei, "A control strategy for permanent magnet synchronous motor wide speed range sensorless system," *Electric Machines and Control Application*, Vol. 44, No. 8, 26–31, 2017.

[13] Yu, J., F. Zhao, F. Gao, *et al.*, "Fuzzy sliding mode observer control for PMSM based on two-stage filter," *Power Electronics*, Vol. 55, No. 1, 9–12, 2021.

[14] Hu, Q. and R. Zhang, "Position Estimation Error Suppression of PMSM Based on complex coefficients sliding mode observer," *Electric Machines and Control*, Vol. 27, No. 12, 41–51, 2023.

[15] Xu, R., Y. Zhang, and H. Wei, "Research on sensorless control of high speed permanent magnet synchronous motor with improved SMO," *Power Electronics*, Vol. 58, No. 2, 30–33, 2024.

[16] Du, S., Y. Liu, Y. Wang, Y. Li, and Z. Yan, "Research on a permanent magnet synchronous motor sensorless anti-disturbance control strategy based on an improved sliding mode observer," *Electronics*, Vol. 12, No. 20, 4188, 2023.

[17] Zhang, G., R. Xiang, G. Wang, H. Zhang, and D. Xu, "Pulse signal injection in stationary reference frame for sensorless PMSM drives," *Proc. CSEE*, Vol. 41, No. 12, 4297–4306, 2021.